LAWRENCE
LIVERMORE
NATIONAL
LABORATORY

LLNL-JRNL-782157

Using a 3D porous flow-through electrode geometry for high rate electrochemical reduction of CO2 to CO in ionic liquid

V. Vedharathinam, Z. Qi, C. Horwood, B. Bourcier, M. Stadermann, J. Biener, M. Biener

July 22, 2019

ACS Catalysis

Using a 3D porous flow-through electrode geometry for high rate electrochemical reduction of CO_2 to CO in ionic liquid

Vedasri Vedharathinam, Zhen Qi, Corie Horwood, Bill Bourcier, Michael Stadermann, Juergen Biener, and Monika Biener**

Lawrence Livermore National Laboratory, Livermore, California 94550, United States

KEYWORDS

Flow-through electrochemistry, ionic liquid, CO_2 reduction, porous electrode

ABSTRACT

Three-dimensional porous flow-through electrodes promise the realization of higher current densities in electrochemical carbon dioxide reduction reaction (CO_2RR) by overcoming mass-transport limitations associated with the diffusion of dissolved CO_2 in the bulk electrolyte. Using an ionic liquid-based electrolyte, $[EMIM]BF_4$, offers the additional benefit of higher CO_2 solubility compared to water based electrolytes. In this work we quantitatively evaluated the effects of flow-driven reactant transport on electrode activity and selectivity for electrochemical CO_2RR in $[EMIM]BF_4$. High surface area porous flow-through electrodes were fabricated by wet-chemical deposition of Ag nanoflowers on commercial macroporous Al foams. At the highest electrolyte flow-through rate of 100 ml min^{-1}, we observed a 70-fold increase in partial CO current density, and 7-fold increase in the faradaic efficiency towards CO, from 10% without flow to 75% with flow. At the same time, the selectivity changed from oxalate as the main product without flow to CO in the electrolyte flow-through configuration. These results demonstrate that the flow-through approach provides a promising path forward to control selectivity and to overcome mass-transport limitations of the electrochemical CO_2RR.

1. INTRODUCTION

Global warming, due to increasing atmospheric CO_2 levels to more than 400 ppm caused by extensive usage of fossil fuels, is one of the most serious problems of the 21st century. The Paris climate agreement urges the world to limit the rising global temperatures to well below 2 °C and recommends achieving net-zero CO_2 emissions globally by 2050[1]. As a consequence, efficient CO_2 conversion technologies that transform CO_2 into useful carbon resources such as industrial chemicals (e.g., CO, HCOOH, C_2H_4, etc.) and fuels (e.g., CH_3OH, CH_4, etc.) are highly sought after, and numerous efforts have been undertaken in the past few decades including biochemical, thermochemical, photochemical and electrochemical CO_2 conversion technologies[2-6]. Among these the electrochemical reduction of carbon dioxide (CO_2RR) represents a promising approach towards artificial carbon recycling due to the use of ambient conditions and the promise of scalability[7], specifically if the transformation is driven with renewable energy sources, like solar energy [8-10].

Extensive research has been done on CO_2RR since the early 90s and summarized elsewhere[3-4, 8, 11-13]. However, the technology still needs to overcome low activity and product selectivity linked to high kinetic barriers and competing hydrogen evolution reaction (HER) in aqueous media. The development of catalysts with higher reactivity and selectivity towards CO_2RR thus remains a key area of research in this field. The high kinetic barrier (overpotential) for CO_2RR, i.e., -1.9 V *vs.* SHE, is due to the large thermodynamic reorganization energy associated with the direct $1e^-$ reduction of linear CO_2 to bent CO_2^{*-}, which is believed to be the rate determining step[14-15]. Another limitation of CO_2RR is the low solubility of CO_2 in water and the pH dependent $CO_{2(dissolved)}$/bicarbonate equilibrium that affects the reaction rate[16-18]. Any increase in the local pH above that of a CO_2 saturated 0.1M $KHCO_3$ electrolyte (pH of 6.8) further decreases local

concentration of dissolved CO_2, and thus the partial CO_2RR current densities[17]. Using ionic liquid based electrolytes is a promising approach to overcome these issues because they generally provide high CO_2 solubility, stabilize the CO_2^{*-} radical anion and suppress the hydrogen evolution reaction (HER)[14-15].

Room temperature ionic liquids (RTILs) are relatively novel liquid salts, solely comprising of an asymmetric organic cation and an inorganic anion. Their exceptional physicochemical properties such as high CO_2 solubility (around 0.10 mol L^{-1} for various imidazolium based ionic liquids at 1 atm, compared to ~ 0.03 mol L^{-1} in water), high intrinsic ionic conductivity, and a wide potential window makes them attractive as solvents for electrochemical CO_2RR[19-21]. For the first time, Zhao et. al, demonstrated the use of a room temperature ionic liquid, 1-n-butyl-3-methylimidazolium hexafluorophosphate ([BMIM]PF_6), as electrolyte for high-pressure electrochemical reduction of supercritical CO_2 and water at lower overpotential using a Cu cathode[22]. Since then, numerous research studies have been undertaken on utilizing RTILs as electrolyte for CO_2RR[15, 22-26]. Recent publications show that imidazolium based ionic liquids, like [EMIM]BF_4, enhance the electrochemical reduction of CO_2 by lowering its overpotential. Rosen et al. reported that the aqueous solution of 18 mol% 1-ethyl-3-methylimidazolium tertrafluoroborate ([EMIM]BF_4) in water decreases the overpotential of the electrochemical reduction of CO_2 to CO on Ag cathodes by ~600 mV, with high faradaic efficiency of 96 % for 7 h[15]. It was hypothesized that the energy barrier of the CO_2 to CO reduction is lowered by the formation of an EMIM-CO_2 complex. Apart from lowering the reaction overpotential, the competing HER was also suppressed by a monolayer of adsorbed cations on the electrode surface[25, 27]. The conversion efficiency of CO_2 to CO on Ag nanoparticle electrocatalyst in [EMIM]BF_4 electrolyte was enhanced by the addition of water when compared to its drier

counterpart[25]. The performance enhancement was due to the hydrolysis of tetrafluoroborate that releases protons when mixed with water. Such water related enhancements in ionic liquids have been reported by various groups[23, 25, 28-29].

Similar to aqueous electrolytes[30-31], the CO_2RR in ionic liquid based electrolytes at high overpotentials becomes controlled by the diffusion of dissolved CO_2 to the electrode/electrolyte interface[29, 32]. Even with the higher CO_2 solubility, the reported maximum current density for CO_2RR in ionic liquid electrolytes remains low, 12 mA cm^{-2} [20], prohibiting an industrial level scale up. Achieving high current densities thus remains one of the major challenges in the commercialization of electrochemical CO_2RR reactors. Many efforts have been devoted to diminishing the activation polarization by discovering efficient catalysts[23, 28, 33-35]. Nevertheless, ohmic and mass transfer polarization are equally responsible for low voltage efficiency. Previous work has shown that the performance of electrochemical reactors can be improved by integrating a flow-through porous electrode design[36-40]. Flowing the electrolyte along the electrode/electrolyte interface reduces the boundary layer thickness (δ), which determines the limiting current density (i_L), as described in equations (2) – (3). Herein, we explore a 3D flow-through electrode geometry for CO_2RR that promises faster mass transport to support high current densities for CO_2 reduction to CO. Our study highlights the importance of reactor design and engineered 3-D porous flow-through electrode to minimize the mass transport related losses, in turn increasing the product flux. To focus on the mass transport aspect of our work, we employed a Ag coated Al foam 3D flow-through cathode as Ag is known for its high selectivity towards CO[15, 35, 41]. We use a [EMIM]BF_4/H_2O (92/8 v/v %) mixture as electrolyte to take advantage of the higher CO_2 solubility of the ionic liquid component, while adding water that serves the purpose of providing enough protons without compromising the CO_2RR selectivity, as described elsewhere[23].

2. RESULTS AND DISCUSSION

2.1. Surface characterization of 3D-Ag nanoflower coated Al foam as flow-through electrode

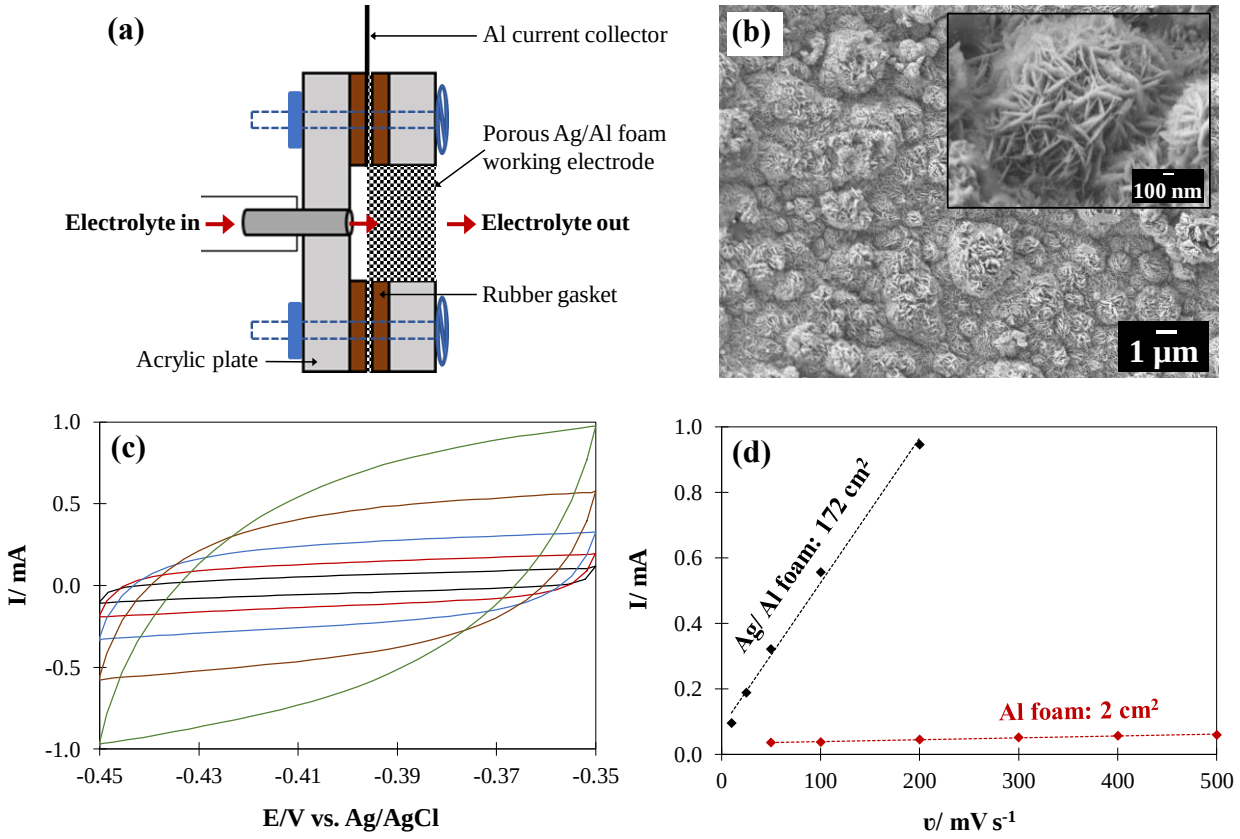

Figure 1. (a) Schematic illustration of the flow-through porous cathode configuration, (b) Low (5000 x) magnification SEM image of the Ag coated Al foam flow-through electrode. Inset showing the nanoflower morphology of the Ag coating at 50000 x, (c) CVs of the 3D Ag coated Al foam working electrode in 0.1M $HClO_4$ at scan rates ranging from 10 to 200 mV s^{-1}, and (d) Al foam working electrode charging current *vs.* scan rate (υ) with and without the Ag nanoflower coating.

The schematic of the flow-through cathode configuration is shown in Figure 1a. Ag catalyst was coated on porous Al foam with an average pore diameter of ~ 650 micron. The morphology of the Ag coated Al foam flow-through electrode was characterized by scanning electron microscope (SEM). The ligaments of the Al foam are uniformly coated with Ag nanoflowers (Figure 1b).

Higher magnification SEM image reveals the nanoflower morphology of the Ag coating, where the nanoflowers consist of approximately 500 nm long and 20 nm thick Ag nanoplatelets. The Ag nanoflower coating increases the electrochemical surface area (ECSA) of the Al foam electrode by a factor of 70, from 2.4 cm^2 for the uncoated Al foam to 176 cm^2 for the Ag coated foam. The roughness factor (defined as the ratio between the ECSA and geometric surface area) of the Ag catalyst coated on Al foam was calculated to be 423.

2.2. Voltammetry study of CO_2 reduction during electrolyte flow-through

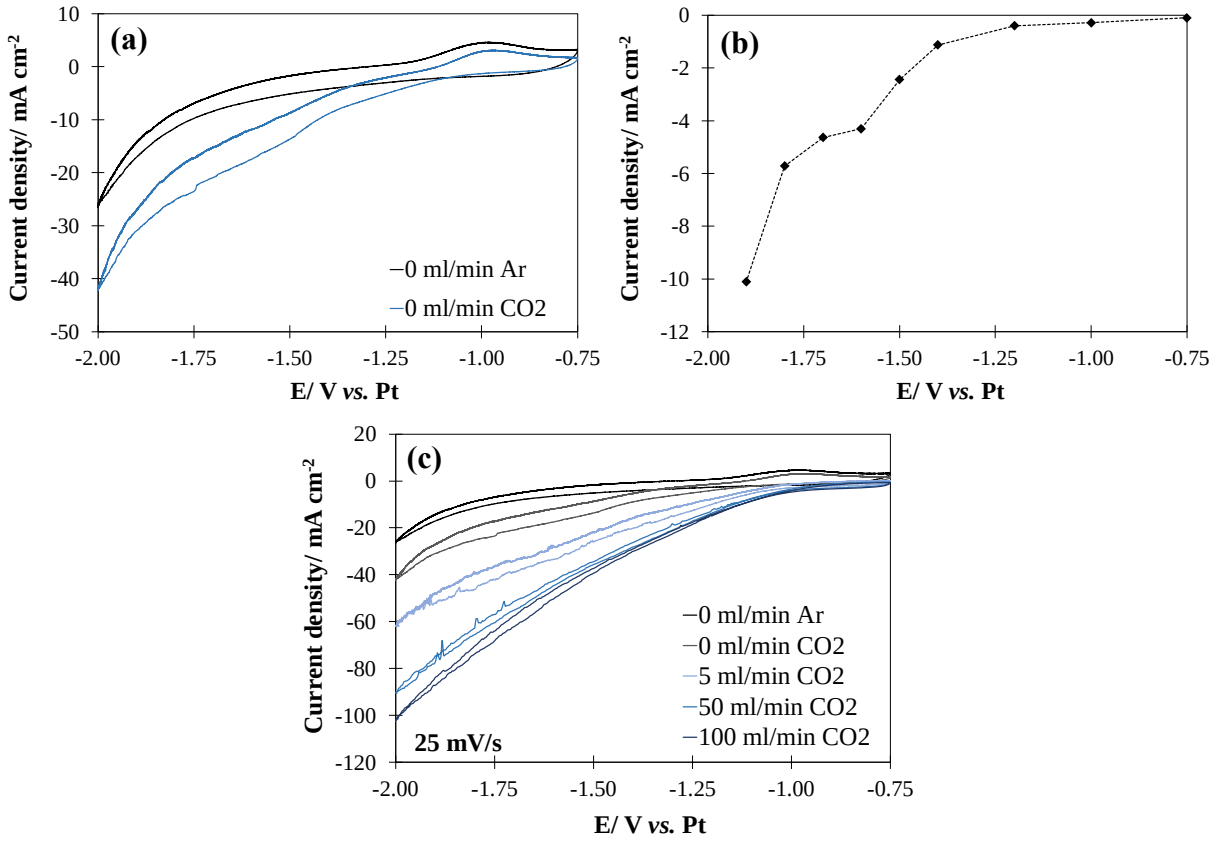

Figure 2. (a) Cyclic voltammograms of the Ag/Al foam electrode at 25 mV s^{-1} in $[EMIM]BF_4/H_2O$ (92/8 v/v%) electrolyte with Ar or CO_2 purging without flow, (b) potential step voltammogram

obtained while CO_2 purging without flow at constant potentials applied for 1 h, and (c) cyclic voltammograms obtained at various electrolyte flow-through rates on Ag/Al foam at 25 mV s^{-1} .

Cyclic voltammetry (CV) performed in Ar or CO_2 saturated [EMIM]BF_4/H_2O (92/8 v/v%) electrolyte mixtures provides first evidence that the 3D-Ag nanoflower coated Al foam electrode described above is an efficient CO_2RR catalyst. First, CVs were recorded without flow (0 ml min^{-1}) at a scan rate of 25 mV s^{-1} in Ar or CO_2 saturated electrolyte (Fig. 2a). The CV collected after Ar purging for 30 min to remove any dissolved oxygen from the electrolyte serves as a baseline as the observed current can be attributed to HER since the electrolyte is void of any CO_2. Upon purging with CO_2 (30 min), an additional electrocatalytic wave was observed between -1.1 V and -1.8 V *vs.* Pt wire indicating the electrochemical reduction of CO_2. The corresponding steady-state current densities obtained by potential step voltammetry (Figure 2b) confirm the onset of the CO_2RR at -1.2V *vs.* Pt. A limiting current plateau is observed at potentials above -1.6V *vs.* Pt implying the onset of CO_2 diffusion limitations without flow. Indeed, CVs performed under flow-through conditions (Figure 2c) show a strong increase in the current density with increasing flow rate from -13.5 mA/cm^2 at 0 ml min^{-1} to -40 mA/cm^2 at 100 ml min^{-1} while the CO_2RR onset potential decreased by 130 mV. This and the fact that the 'plateau' like CV feature in the potential region of -1 V to -1.8 V *vs.* Pt wire changes into a more 'linear' response with increasing electrolyte flow-through rate, indicate improved mass-transport kinetics, as seen in various electrochemical flow systems. The decrease in on-set potential and increase in CO_2 reduction current density can be attributed to the decrease in boundary layer thickness when the electrolyte is flown through the porous cathode. Similar results were predicted by Singh et al. for the CO_2RR in aqueous medium, where their model predicted the decrease in polarization loss with decreasing boundary layer thickness[17]. Hence, our experiments support the notion that the electrochemical CO_2RR in

[EMIM]BF_4 (92/8 v/v%) electrolyte becomes diffusion limited for higher current densities/potentials (despite the higher CO_2 solubility in EMIM]BF_4) and that the CO_2 reduction current can be enhanced by using a flow-through electrode geometry.

2.3. Electrochemical CO_2 reduction and product analysis

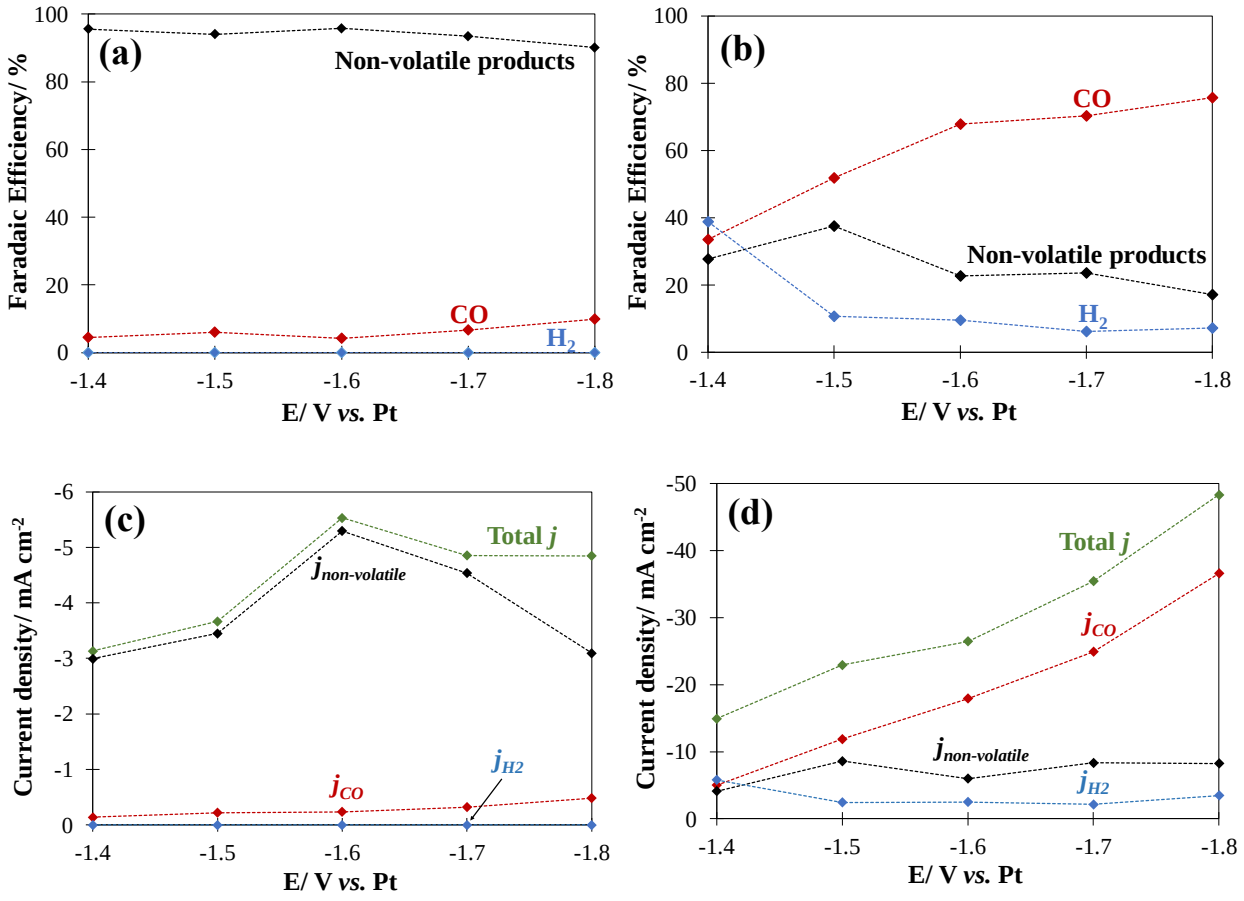

Figure 3. Faradaic efficiency of CO_2 reduction products on a Ag coated Al foam electrode at various cell potentials ranging from -1.4 V to -1.8 V *vs.* Pt in [EMIM]BF_4/H_2O (92/8 v/v%) at electrolyte flow-through rates of (a) 0 ml min^{-1} and (b) 100 ml min^{-1}. Change in partial current density of products (CO, non-volatile products, and H_2) calculated from the faradaic efficiency at

electrolyte flow-through rates of (c) 0 ml min^{-1}, and (d) 100 ml min^{-1}. Note the dramatic change in selectivity and current density w/ electrolyte flow.

To measure the effect of forced electrolyte flow on the CO_2RR rate and product selectivity, we performed constant potential experiments in the range of -1.4 V to -1.8 V *vs.* Pt (Figures 3a – 3d). The only gaseous products detected by GC were CO and H_2, while a small amount (too small for quantitative analysis) of a white precipitate was found on the electrode surface and in the electrolyte. Without flow (0 ml min^{-1}), the current density was low (< 6 mA cm^{-2} within -1.4 V to -1.8 V *vs.* Pt), and j_{CO} accounts only for a small fraction (< 10%) of the experimentally observed current density (Figure 3c). Surprisingly no H_2 was detected by GC under static conditions over the entire cell potential range tested. The corresponding FEs are shown in Figure 3a. The non-accounted current density under static condition (90%) is attributed to the formation of non-volatile CO_2RR products non-detectable by GC (see IR and NMR analysis in SI).

Flowing the electrolyte through the porous electrode (100 ml min^{-1}) dramatically increases j_{total}, j_{CO}, and FE_{CO}, as seen in Figures 3b and 3d : The maximum current density increased by a factor of ~10, from ~5.5 mA cm^{-2} to 48 mA cm^{-2}; j_{CO} increased from 0.5 mA cm^{-2} without flow to 36.6 mA cm^{-2} at 100 ml min^{-1}, a 73-fold increase; FE_{CO} and FE_{H2} increased to 75 % and 10 % at -1.8 V *vs.* Pt, respectively. The product selectivity changes from non-volatile CO_2RR products as the main products without electrolyte flow to CO at 100 ml min^{-1}. Flowing the electrolyte through the electrode does not suppress the formation of the non-volatile products as $j_{non\text{-}volatile}$ increases from ~3 mA cm^{-2} without flow to ~8 mA cm^{-2} at 100 ml min^{-1}, but the increase in $j_{non\text{-}volatile}$ is small (2.7-fold) compared to the 73-fold increase in j_{CO}. Another effect of flow is the potential dependence of current density and product selectivity: Without flow (Figure 3c), the current density only weakly depends on the applied potential (less than a factor of 2 within the applied potential range

of -1.4 V and -1.8 V *vs.* Pt). The "plateau" like maximum of ~5.5 mA cm^{-2} at -1.6 V *vs.* Pt indicates that the system becomes diffusion limited under these conditions. By contrast, at an electrolyte flow-through rate of 100 ml min^{-1} the current density increased monotonically with the applied potential, and the maximum current density of ~50 mA cm^{-2} is observed at the highest applied potential, -1.8 V *vs.* Pt (Figure 3d). The absence of a limiting current plateau suggests that the system never becomes diffusion limited under applied flow-through conditions. $FE_{non\text{-}volatile}$ with applied flow decreases to 40 % and 15% at -1.5 V and -1.8 V *vs.* Pt, respectively, due to the much faster increase of j_{CO} compared to $j_{non\text{-}volatile}$ under flow conditions. The up to 8-fold increase in FE_{CO} with electrolyte flow through the porous electrode seems to be a direct consequence of the improved, flow-driven mass-transport of dissolved CO_2 to the internal surface area of the porous electrode. Similarly, the increase in FE_{H2} with flow, from 0 % without flow to 10 % at 100 ml min^{-1}, may also be a consequence of flow-driven mass transport limiting the increase of the local pH in confined pores thus effectively decreasing the overpotential for HER in the presence of flow. These observations suggest that flowing the electrolyte through the porous electrode helps to remove the product CO from the pores thus opening catalytic sites for further CO_2RR and making CO the main product. To identify the non-volatile CO_2RR product that is the main product without flow, we analyzed the white precipitate using fourier transform infrared spectroscopy (FTIR) and the ionic liquid electrolyte using nuclear magnetic resonance spectroscopy (NMR). The white precipitate collected after 10 h of CO_2 electrolysis without flow at -1.7 V in [EMIM]BF_4/H_2O (92/8 v/v%) was rinsed with acetonitrile three times in a centrifuge, and dissolved in DMSO for further FTIR analysis. The two peaks at 1620 cm^{-1} and 1320 cm^{-1} can be assigned to the asymmetric and symmetric O-C-O stretching modes (Figure S2) of oxalate. The 13-C NMR analysis before and after CO_2RR did not show any other products in the liquid phase. As reported

in the literature, the formation of oxalate is the result of dimerization of CO_2^{*-} [26]. Observing oxalate as the main product without flow is surprising as CO is typically the main CO_2RR product on Ag foils[15, 25, 27]. We speculate that the Ag nanoflower morphology confines the CO_2^{*-} radical reaction intermediate thus facilitating its coupling towards oxalate.

Flowing electrolyte through the porous electrode changes the product distribution dramatically: Instead of the non-volatile product at 0 ml min^{-1}, CO becomes the main product with flow (100 ml min^{-1}). The dramatic increase in reactivity and the change in selectivity towards CO formation with electrolyte flow-through can be attributed to two effects: 1) The flowing electrolyte facilitates the release of the product CO from the catalyst surface, thus freeing up active sites for further reduction of CO_2 and 2) the local pH in the catalyst pores stay lower with fresh electrolyte flowing through the pores thus providing a higher proton concentration for the reduction of the CO_2^{*-} radical anion to produce CO[26].

$$CO_2^{*-} + 2H^+ + e^- \rightarrow CO + H_2O \quad (1)$$

Indeed, the hydrogen partial current density is higher with flow than without flow thus supporting the idea of a lower pH in the catalyst pores under flow conditions.

Although we never reached the limiting current regime under flow-through conditions (Figure 3d), it is nevertheless instructive to analyze the observed maximum current density in terms of a boundary layer thickness. Under limiting current conditions, when the CO_2 concentration in the electrolyte at the electrode surface approaches 'zero', the increase in potential no longer leads to any increase in the current density. Using Fick's law of diffusion, the limiting current density is described by

$$i_L = zF\frac{D}{\delta_D}C_b \quad (2)$$

where z is the number of electrons transferred (CO = 2 e^-), F is Faraday's constant (96485 C mol^{-1}), D is the diffusion coefficient of CO_2 in [EMIM]BF_4/H_2O (92/8 v/v%) (3 x 10^{-6} cm^2 s^{-1})[29], C_b is the concentration of CO_2 in [EMIM]BF_4/H_2O (92/8 v/v%) (9 x 10^{-5} mol cm^{-3})[29], and δ_D is the boundary layer thickness (cm). For the flow conditions employed in this work (0 to 100 ml min^{-1}), a pore diameter d_p of 650 µm, and viscosity of (0.396 cm^2/s)[29] for the EMIM]BF_4/H_2O electrolyte, the Reynolds number is between 0.2 and 41, well within the laminar flow regime (Figure S4). It is thus safe to assume a parabolic flow profile with a no-slip boundary at the electrode surface and the highest linear flow velocity at the center of the tubular channel. Under these conditions for Poiseuille flow with the Leveque approximation, the boundary layer thickness (δ) scales with the cube root of the inverse mean flow velocity U in m s^{-1}[42-44]:

$$\delta = 1.607 \sqrt[3]{\frac{d_p D L}{\mathrm{U}}} \tag{3}$$

$$\mathrm{U} = \frac{Q}{A_{geometric}\,\epsilon} \tag{4}$$

where d_p is the pore diameter in cm, D is the diffusion coefficient of CO_2 in [EMIM]BF_4/H_2O (92/8 v/v%) (3 x 10^{-6} cm^2 s^{-1}), the pore length L is taken as the thickness of the porous electrode in cm (0.2), and U is the mean flow velocity in cm s^{-1}, Q is the electrolyte flow rate from the recirculation pump in ml min^{-1}, $A_{geometric}$ is the geometric area of the electrode in cm and ϵ is the porosity of the flow-through electrode (0.9).

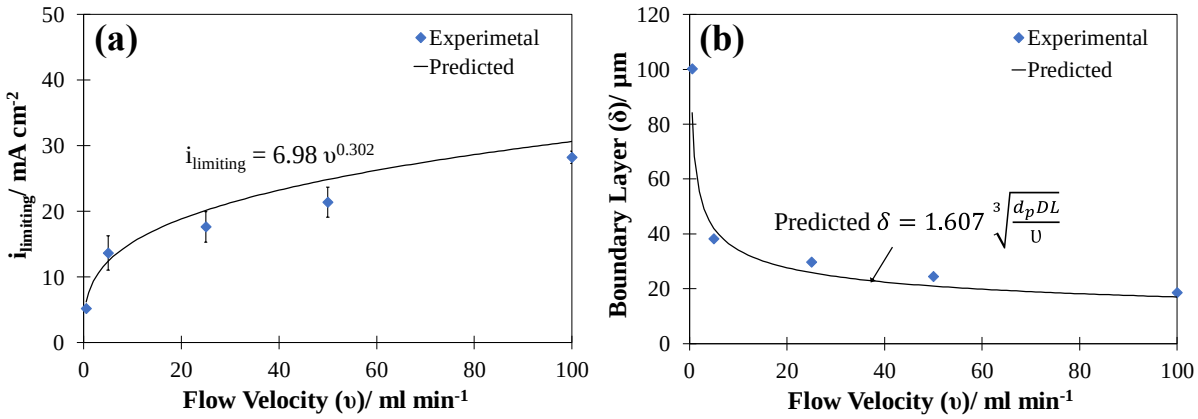

Figure 4. Effect of electrolyte flow-through rate on CO_2RR using Ag modified Al foam electrode in [EMIM]BF_4/H_2O (92/8 v/v) at -1.7 V *vs.* Pt: Predicted and experimental limiting current density (a) and boundary layer thickness (b).

The effect of the electrolyte flow-through rate on the CO_2RR current density and boundary layer thickness was studied in more detail using chronoamperometry at -1.7 V *vs.* Pt (Figures 4 a, b). The experiments were repeated three times and the average current density for each flow-through rate is plotted in Figure 4(a). The increase in current density with increasing flow-through rate from 0.5 ml min^{-1} to 100 ml min^{-1} follows a power law with an exponent of 0.3. This value is close to the 1/3rd (0.33) power dependence of limiting current density on flow rate for various porous electrodes predicted by Newman et. al.[45-46] and others[47-50]. Thus, even though we never observed a limiting current plateau under flow conditions (Figure 4), the experimentally observed current density-flow-through rate dependence is in good agreement with the prediction of the limiting current analysis outlined above. The increase in current density with increasing electrolyte flow-through rate may thus be attributed to the decrease in the boundary layer thickness δ, under flow conditions, from 100 µm at 0.5 ml min $^{-1}$ to 18 µm at 100 ml min $^{-1}$ (Figure 4b)

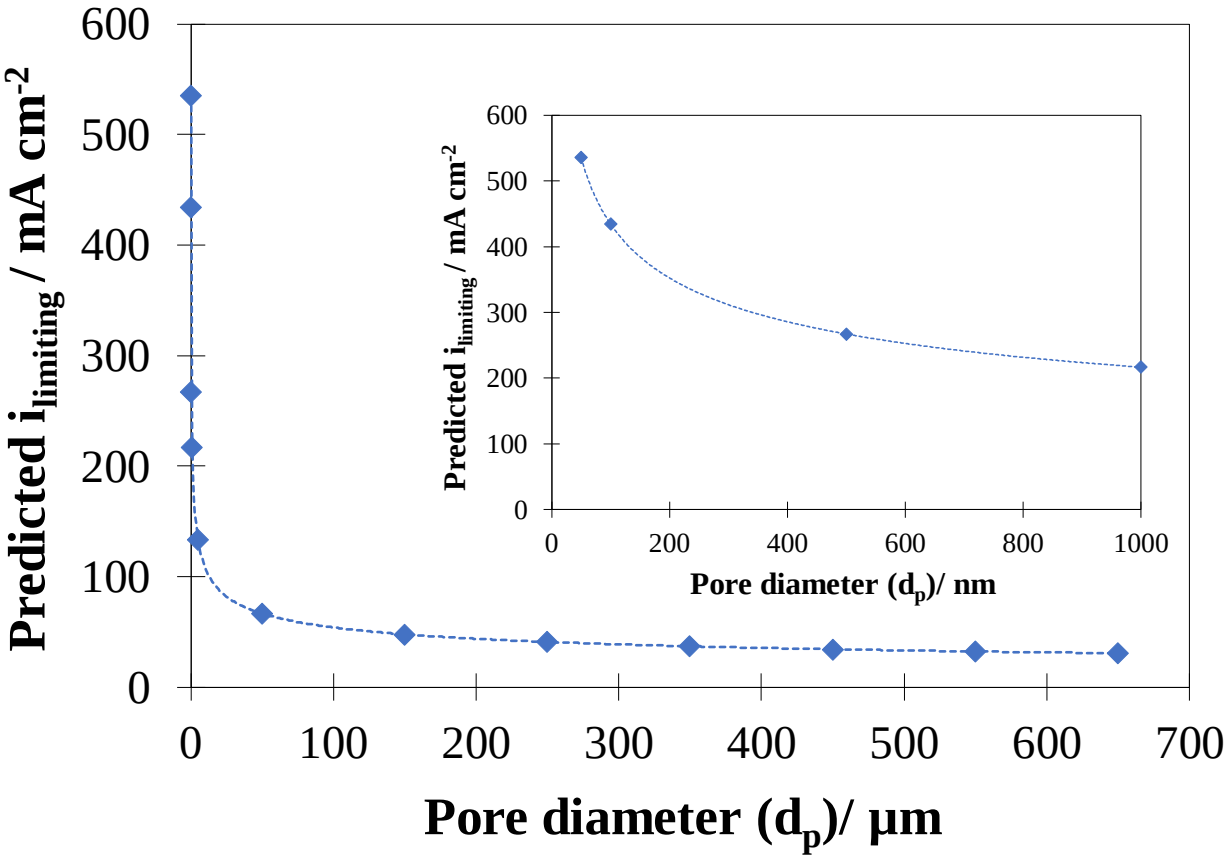

Figure 5. Predicted limiting current density (i_L) with varying pore diameter (d_p). Inset shows the pore diameter in the nm range.

The results also suggest that the current density of the CO_2RR can be further enhanced by designing porous flow-through electrodes with smaller flow-through channels that result in higher flow velocities. According to Eq. 3, the boundary layer thickness that controls the limiting current density also scales with the cube root of the pore diameter d_p. Combining Eq. 2 and 3, the predicted limiting current density increases with decreasing pore diameter of the flow-through electrode by an order of magnitude, from 31 mA cm^{-2} for 650 µm pores to 535 mA cm^{-2} for 0.05 µm pores. The increased limiting current density however comes at the cost of a higher flow resistance through the porous electrode. Nevertheless, the analysis suggests that mass-transport limitations of the

CO_2RR can be further improved by finding the optimum compromise between reduced boundary layer thickness and increasing flow resistance losses that come with smaller pores. Design of high surface area and mechanically robust nanoporous electrodes for CO_2RR is thus a promising route to achieve high current densities.

3. CONCLUSION

In this study, we demonstrate that forcing an electrolyte through a porous cathode in a CO_2RR setup not only increases the current density but also changes the product selectivity. For our Ag nanoflower coated microporous aluminum electrodes, the selectivity changes from oxalate without flow to CO as the main product in the electrolyte flow-through configuration. At the same time the total current density of CO increases by a factor of 10 when the flow-through rates were increased from 0 ml min^{-1} to 100 ml min^{-1}. Using forced flow conditions allows us to reduce the mass transport limitations by decreasing the boundary layer thickness, and thus to utilize the high internal surface area of the Ag nanoflower catalyst more efficiently. Our results demonstrate that the flow-through approach provides a promising path forward to control selectivity and to overcome mass-transport limitations of the electrochemical CO_2RR.

AUTHOR INFORMATION

Corresponding Author

* biener3@llnl.gov; * vedharathina1@llnl.gov;

ACKNOWLEDGMENT

The authors are grateful for the support of this research under the auspices of the U.S. Department of Energy under Contract DE-AC52-07NA27344, through LDRD award 17-LW-013. IM release # LLNL-JRNL-782157.

REFERENCES

1. *Reaching Net-zero Carbon Emissions from Harder-to-abate Sectors by Mid-Century*; Energy Transitions Commission: 2018.
2. Tu, W.; Zhou, Y.; Zou, Z., Photocatalytic Conversion of CO_2 into Renewable Hydrocarbon Fuels: State-of-the-Art Accomplishment, Challenges, and Prospects. *Adv. Mater.* **2014,** *26* (27), 4607-4626.
3. Whipple, D. T.; Kenis, P. J. A., Prospects of CO_2 Utilization via Direct Heterogeneous Electrochemical Reduction. *J. Phys. Chem. Lett.* **2010,** *1* (24), 3451-3458.
4. Zheng, T.; Jiang, K.; Wang, H., Recent Advances in Electrochemical CO_2 to CO Conversion on Heterogeneous Catalysts. *Adv. Mater.* **2018,** *30* (48), 1802066.
5. Lee, J.-S.; Lee, J.-P., Review of Advances in Biological CO_2 Mitigation Technology. *Biotechnol. Bioprocess Eng.* **2003,** *8* (6), 354.
6. Roy, S. C.; Varghese, O. K.; Paulose, M.; Grimes, C. A., Toward Solar Fuels: Photocatalytic Conversion of Carbon Dioxide to Hydrocarbons. *ACS Nano* **2010,** *4* (3), 1259-1278.
7. Savéant, J.-M., Molecular Catalysis of Electrochemical Reactions. Mechanistic Aspects. *Chem. Rev.* **2008,** *108* (7), 2348-2378.
8. Kauffman, D. R.; Thakkar, J.; Siva, R.; Matranga, C.; Ohodnicki, P. R.; Zeng, C.; Jin, R., Efficient Electrochemical CO_2 Conversion Powered by Renewable Energy. *ACS Appl. Mater. Interfaces* **2015,** *7* (28), 15626-15632.
9. Centi, G.; Quadrelli, E. A.; Perathoner, S., Catalysis for CO_2 Conversion: A Key Technology for Rapid Introduction of Renewable Energy in the Value Chain of Chemical Industries. *Energy Environ. Sci.* **2013,** *6* (6), 1711-1731.
10. Zhan, Z.; Kobsiriphat, W.; Wilson, J. R.; Pillai, M.; Kim, I.; Barnett, S. A., Syngas Production by Coelectrolysis of CO_2/H_2O: The Basis for a Renewable Energy Cycle. *Energy Fuels* **2009,** *23* (6), 3089-3096.
11. Spinner, N. S.; Vega, J. A.; Mustain, W. E., Recent Progress in the Electrochemical Conversion and Utilization of CO_2. *Catal. Sci. Technol.* **2012,** *2* (1), 19-28.
12. Gattrell, M.; Gupta, N.; Co, A., A Review of the Aqueous Electrochemical Reduction of CO_2 to Hydrocarbons at Copper. *J. Electroanal. Chem.* **2006,** *594* (1), 1-19.
13. Albo, J.; Alvarez-Guerra, M.; Castaño, P.; Irabien, A., Towards the Electrochemical Conversion of Carbon Dioxide into Methanol. *Green Chem.* **2015,** *17* (4), 2304-2324.
14. Vassiliev, Y. B.; Bagotzky, V. S.; Khazova, O. A.; Mayorova, N. A., Electroreduction of Carbon Dioxide: Part II. The Mechanism of Reduction in Aprotic Solvents. *J. Electroanal. Chem. Interfacial Electrochem.* **1985,** *189* (2), 295-309.

15. Rosen, B. A.; Salehi-Khojin, A.; Thorson, M. R.; Zhu, W.; Whipple, D. T.; Kenis, P. J.; Masel, R. I., Ionic Liquid-Mediated Selective Conversion of CO_2 to CO at Low Overpotentials. *Science* **2011,** *334* (6056), 643-4.
16. Hashiba, H.; Weng, L.-C.; Chen, Y.; Sato, H. K.; Yotsuhashi, S.; Xiang, C.; Weber, A. Z., Effects of Electrolyte Buffer Capacity on Surface Reactant Species and the Reaction Rate of CO_2 in Electrochemical CO_2 Reduction. *J. Phys. Chem. C* **2018,** *122* (7), 3719-3726.
17. Singh, M. R.; Clark, E. L.; Bell, A. T., Effects of Electrolyte, Catalyst, and Membrane Composition and Operating Conditions on the Performance of Solar-Driven Electrochemical Reduction of Carbon Dioxide. *Phys. Chem. Chem. Phys.* **2015,** *17* (29), 18924-36.
18. Chen, Y.; Lewis, N. S.; Xiang, C., Modeling and Simulation of the Spatial and Light-Intensity Dependence of Product Distributions in an Integrated Photoelectrochemical CO_2 Reduction System. *ACS Energy Lett.* **2016,** *1* (1), 273-280.
19. Torralba-Calleja, E.; Skinner, J.; Gutiérrez-Tauste, D., CO_2 Capture in Ionic Liquids: A Review of Solubilities and Experimental Methods. *J. Chem.* **2013,** *2013*, 16.
20. Feng, J.; Zeng, S.; Feng, J.; Dong, H.; Zhang, X., CO_2 Electroreduction in Ionic Liquids: A Review. *Chin. J. Chem.* **2018,** *36* (10), 961-970.
21. Alvarez-Guerra, M.; Albo, J.; Alvarez-Guerra, E.; Irabien, A., Ionic Liquids in the Electrochemical Valorisation of CO_2. *Energy Environ. Sci.* **2015,** *8* (9), 2574-2599.
22. Zhao, G.; Jiang, T.; Han, B.; Li, Z.; Zhang, J.; Liu, Z.; He, J.; Wu, W., Electrochemical Reduction of Supercritical Carbon Dioxide in Ionic Liquid 1-n-Butyl-3-Methylimidazolium Hexafluorophosphate. *J. Supercrit. Fluids* **2004,** *32* (1), 287-291.
23. Huan, T. N.; Simon, P.; Rousse, G.; Genois, I.; Artero, V.; Fontecave, M., Porous Dendritic Copper: An Electrocatalyst for Highly Selective CO_2 Reduction to Formate in Water/Ionic Liquid Electrolyte. *Chem. Sci.* **2017,** *8* (1), 742-747.
24. Papasizza, M.; Cuesta, A., In-situ Monitoring using ATR-SEIRAS of the Electrocatalytic Reduction of CO_2 on Au in an Ionic Liquid/Water Mixture. *ACS Catal.* **2018,** *8* (7), 6345-6352.
25. Rosen, B. A.; Zhu, W.; Kaul, G.; Salehi-Khojin, A.; Masel, R. I., Water Enhancement of CO_2 Conversion on Silver in 1-Ethyl-3-Methylimidazolium Tetrafluoroborate. *J. Electrochem. Soc.* **2012,** *160* (2), H138-H141.
26. Sun, L.; Ramesha, G. K.; Kamat, P. V.; Brennecke, J. F., Switching the Reaction Course of Electrochemical CO_2 Reduction with Ionic Liquids. *Langmuir* **2014,** *30* (21), 6302-8.
27. Rosen, B. A.; Haan, J. L.; Mukherjee, P.; Braunschweig, B.; Zhu, W.; Salehi-Khojin, A.; Dlott, D. D.; Masel, R. I., In Situ Spectroscopic Examination of a Low Overpotential Pathway for Carbon Dioxide Conversion to Carbon Monoxide. *J. Phys. Chem. C* **2012,** *116* (29), 15307-15312.
28. Oh, Y.; Hu, X., Ionic Liquids Enhance the Electrochemical CO_2 Reduction Catalyzed by MoO_2. *Chem. Commun.* **2015,** *51* (71), 13698-701.
29. Rudnev, A. V.; Fu, Y. C.; Gjuroski, I.; Stricker, F.; Furrer, J.; Kovacs, N.; Vesztergom, S.; Broekmann, P., Transport Matters: Boosting CO_2 Electroreduction in Mixtures of [BMIm][BF_4]/Water by Enhanced Diffusion. *ChemPhysChem* **2017,** *18* (22), 3153-3162.
30. David, R.; Mark, M.; Chao, W., Mass transport modelling for the electroreduction of CO_2 on Cu nanowires. *Nanotechnology* **2018,** *29* (4), 044001.

31. Kotb, Y.; Fateen, S.-E. K.; Albo, J.; Ismail, I., Modeling of a Microfluidic Electrochemical Cell for the Electro-Reduction of CO_2 to CH_3OH. *J. Electrochem. Soc.* **2017,** *164* (13), E391-E400.
32. Tanner, E. E. L.; Batchelor-McAuley, C.; Compton, R. G., Carbon dioxide Reduction in Room-Temperature Ionic Liquids: The Effect of the Choice of Electrode Material, Cation, and Anion. *J. Phys. Chem. C* **2016,** *120* (46), 26442-26447.
33. Watkins, J. D.; Bocarsly, A. B., Direct Reduction of Carbon Dioxide to Formate in High-Gas-Capacity Ionic Liquids at Post-Transition-Metal Electrodes. *ChemSusChem* **2014,** *7* (1), 284-290.
34. Zhu, Q.; Ma, J.; Kang, X.; Sun, X.; Liu, H.; Hu, J.; Liu, Z.; Han, B., Efficient Reduction of CO2 into Formic Acid on a Lead or Tin Electrode using an Ionic Liquid Catholyte Mixture. *Angew. Chem. Int. Ed* **2016,** *128* (31), 9158-9162.
35. Reche, I.; Gallardo, I.; Guirado, G., Electrochemical Studies of CO_2 in Imidazolium Ionic Liquids using Silver as a Working Electrode: A Suitable Approach for Determining Diffusion Coefficients, Solubility Values, and Electrocatalytic Effects. *RSC Adv.* **2014,** *4* (110), 65176-65183.
36. Lessner, P. M.; McLarnon, F. R.; Winnick, J.; Cairns, E. J., Aqueous Polysulphide Flow-through Electrodes: Effects of Electrocatalyst and Electrolyte Composition on Performance. *J. Appl. Electrochem.* **1992,** *22*, 927-934.
37. Cheng, W. L.; Erbay, C.; Sadr, R.; Han, A., Dynamic Flow Characteristics and Design Principles of Laminar Flow Microbial Fuel Cells. *Micromachines* **2018,** *9* (10).
38. Weekes, D. M.; Salvatore, D. A.; Reyes, A.; Huang, A.; Berlinguette, C. P., Electrolytic CO_2 Reduction in a Flow Cell. *Acc. Chem. Res.* **2018,** *51* (4), 910-918.
39. Widner, R. C.; Sousa, M. B.; Bertazzoli, R., Electrolytic Removal of Lead using a Flow-through Cell with a Reticulated Vitreous Carbon Cathode. *J. Appl. Electrochem.* **1998,** *28*, 201-207.
40. Monroe, M. M.; Lobaccaro, P.; Lum, Y.; Ager, J. W., Membraneless Laminar Flow Cell for Electrocatalytic CO_2 Reduction with Liquid Product Separation. *J. Phys. D: Appl. Phys.* **2017,** *50* (15).
41. Lau, G. P.; Schreier, M.; Vasilyev, D.; Scopelliti, R.; Gratzel, M.; Dyson, P. J., New Insights into the Role of Imidazolium-Based Promoters for the Electroreduction of CO_2 on a Silver Electrode. *J. Am. Chem. Soc.* **2016,** *138* (25), 7820-3.
42. Braff, W. A.; Buie, C. R.; Bazant, M. Z., Boundary Layer Analysis of Membraneless Electrochemical Cells. *J. Electrochem. Soc.* **2013,** *160* (11), A2056-A2063.
43. Braff, W. A.; Bazant, M. Z.; Buie, C. R., Membrane-less Hydrogen Bromine Flow Battery. *Nat. Commun.* **2013,** *4*, 2346.
44. Poiseuille Flow with Leveque Approximation. In *MIT Class Notes*, Massachusetts Institute of Technology, 2014.
45. Selman, J. R.; Newman, J., Free-Convection Mass Transfer with a Supporting Electrolyte. *J. Electrochem. Soc.* **1971,** *118* (7), 1070-1078.
46. Fickett, A. P., Electrochemical Systems *AlChE J.* **1973,** *19* (4), 879-879.
47. You, X.; Ye, Q.; Cheng, P., The Dependence of Mass Transfer Coefficient on the Electrolyte Velocity in Carbon Felt Electrodes: Determination and Validation. *J. Electrochem. Soc.* **2017,** *164* (11), E3386-E3394.

48. Tobias, C. W.; Eisenberg, M.; Wilke, C. R., Fiftieth Anniversary: Diffusion and Convection in Electrolysis - A Theoretical Review. *J. Electrochem. Soc.* **1952,** *99* (12), 359C-365C.
49. Scott, K.; Lobato, J., Determination of a Mass-Transfer Coefficient using the Limiting-Current Technique. *Chem. Educ.* **2002,** *7* (4), 214-219.
50. Quiroz, M.; A. Martinez-Huitle, U.; Martinez-Huitle, C. A., Mass Transfer Measurements in a Parallel Disk Cell Using the Limiting Current Technique. *J. Mex. Chem. Soc.* **2005,** *49*, 279-283.